Bose-Fermi mixtures in an optical lattice

K. Sengupta,[1] N. Dupuis,[2,3,4] and P. Majumdar[5,6]

[1]*Theoretical Condensed Matter Physics Division and Center for Applied Mathematics and Computational Science,*
Saha Institute of Nuclear Physics, 1/AF Bidhannagar, Kolkata-700064, India
[2]*Department of Mathematics, Imperial College, 180 Queen's Gate, London SW7 2AZ, United Kingdom*
[3]*Laboratoire de Physique des Solides, Université Paris-Sud, CNRS, UMR 8502, F-91405 Orsay Cedex, France*
[4]*LPTMC, CNRS-UMR 7600, Université Pierre et Marie Curie, 75252 Paris Cédex 05, France*
[5]*Cavendish Laboratory, Cambridge University, Madingley Road, Cambridge CB3 0HE, United Kingdom*
[6]*Harish-Chandra Research Institute, Chhatnag Road, Jhunsi, Allahabad 211019, India*

We study an atomic Bose-Fermi mixture with unpolarized fermions in an optical lattice. We obtain the Mott ground states of such a system in the limit of the deep optical lattice and discuss the effect of quantum fluctuations on these states. We also study the superfluid-insulator transitions of bosons and metal-insulator transition of fermions in such a mixture within a slave-rotor mean-field approximation, and obtain the corresponding phase diagram. We discuss experimental implications of our results.

I. INTRODUCTION

Recent experiments on ultracold trapped atomic gases have opened a new window into the phases of quantum matter [1]. A gas of bosonic atoms in an optical or magnetic trap has been reversibly tuned between superfluid (SF) and insulating ground states by varying the strength of a periodic potential produced by standing optical waves [1,2]. This transition has been explained on the basis of the Bose-Hubbard model with on-site repulsive interactions and hopping between nearest neighboring sites of the lattice [3–7]. Further, theoretical studies of bosonic atoms with spin and/or pseudospin have also been undertaken [8–11]. These studies have revealed a variety of interesting Mott phases and superfluid-insulating transitions in these systems. On the fermionic side, the experimental studies have mainly concentrated on the observation of paired superfluid states [12] and the BCS-BEC crossover in such systems near a Feshbach resonance [13].

More recently, it has been possible to generate mixtures of fermionic and bosonic atoms in a trap [14,15]. Initially, the main focus of such experimental studies was to generate quantum degenerate Fermi gases, through sympathetic cooling with bosons. However, a host of theoretical studies followed soon, which established such Bose-Fermi mixtures to be interesting physical systems in their own right [16–20], exhibiting exciting Mott phases in the presence of an optical lattice. In all of these works, the spin of the fermions in the mixture is taken to be frozen out due to the presence of the magnetic trap. However, more recent works reported in Refs. [21,22] considered a Bose-Fermi mixture in an optical trap, where the spins of the fermions can be dynamical degrees of freedom [23]. It has been shown in Ref. [21] that the interaction between the bosons and the fermions in such a mixture can enhance the *s*-wave pairing instability of the fermions.

In this work, we consider a Bose-Fermi mixture in an optical trap and in the presence of an optical lattice and study the Mott phases and the metal–superfluid-insulator transition

for the fermions and bosons of such a mixture using a slave-rotor mean-field theory [24]. The motivation for such a study is twofold. First, it has been shown in Ref. [18] that the Mott phases of Bose-Fermi mixtures in a magnetic trap are interesting in their own right. In the present study, we chart out the Mott phases of the Bose-Fermi mixture in an optical trap, where the fermion spins are dynamical degrees of freedom, in the deep lattice limit for a wide range of parameters. As expected, we find that the corresponding Mott phases obtained are much richer than their counterparts studied in Ref. [18]. Second, the metal–superfluid-insulator transition of the fermions and bosons in such an interacting Bose-Fermi mixture has not been studied before. Here we develop a self-consistent slave-rotor mean-field theory to study such a transition for the Mott phases which do not have density-wave order with broken translational symmetry and use it to obtain at least a qualitative understanding of the effect of interaction between the fermions and the bosons on the metal–superfluid-insulator transition.

In what follows, we shall assume that the atoms are confined using an optical trap so that fermion spins are not frozen out. We shall, however, ignore the effect of the harmonic trap potential which is a standard approximation used extensively in the literature [25]. The starting point of our study is the Bose-Fermi Hubbard Hamiltonian that has been developed earlier, with similar approximation regarding the trap potential, from underlying microscopic dynamics of the atoms in the presence of an optical lattice [17]

$$\mathcal{H} = \mathcal{H}_F + \mathcal{H}_B + \mathcal{H}_{FB}, \tag{1}$$

$$\mathcal{H}_F = -t_F \sum_{\langle ij \rangle \sigma} (c_{i\sigma}^\dagger c_{j\sigma} + \text{H.c.}) - \mu_F \sum_{i\sigma} n_{i\sigma}^F + U_{FF} \sum_i n_{i\uparrow}^F n_{i\downarrow}^F, \tag{2}$$

$$\mathcal{H}_B = -t_B \sum_{\langle ij \rangle \sigma} (b_i^\dagger b_j + \text{H.c.}) - \mu_B \sum_i n_i^B + \frac{U_{BB}}{2} \sum_i n_i^B(n_i^B - 1), \tag{3}$$

$$\mathcal{H}_{FB} = U_{FB} \sum_{i\sigma} n_{i\sigma}^F n_i^B. \qquad (4)$$

Here $c_{i\sigma}$ is the fermionic destruction operator with spin σ $= \uparrow, \downarrow$ at site i, b_i represents the bosonic destruction operator at site i, $n^{F(B)}$ denotes fermion (boson) number operators, $t_{F(B)}$ and $\mu_{F(B)}$ are nearest neighbor hopping matrix elements and chemical potentials for the fermions (bosons), U_{BB} and U_{FF} are the on-site Hubbard repulsion for bosons and fermions, respectively, and U_{FB} denotes the relative interaction strength between the bosons and the fermions. In what follows, we shall take the bosons and the fermions to have fixed chemical potentials $\mu_{B(F)}$ and same on-site repulsion U_{BB} $=U_{FF}=U$ and consider $\lambda = U_{FB}/U$ and $\eta = t_F/t_B$ as parameters which can be freely varied. The justification of this choice is briefly outlined in Sec. II. Further, we shall only deal with the case of a square bipartite lattice in this work since this is simplest to realize experimentally.

The organization of the rest of the paper is as follows. In the next section, we identify the Mott phases of Eq. (1). Next, in Sec. III, we introduce the slave-rotor formalism and use it within a mean-field approximation to study the metal–superfluid-insulator transition of the Bose-Fermi Hubbard model [Eq. (1)]. This is followed by a discussion of possible experiments in Sec. IV. A comparison of the Mott-Hubbard phase diagram obtained using the projection operator technique with those obtained from mean-field theories [3,5,6] and standard strong coupling expansions [26] is given in the Appendix.

II. MOTT PHASES

In this section, we chart out the Mott phases of the Bose-Fermi system. To do this, we first obtain the phases of the system in the Mott limit ($t_B=t_F=0$) and then obtain fluctuation corrections over these states to $O(t_{B(F)}^2/U^2)$.

Before obtaining the Mott phases for the Bose-Fermi mixture, let us look briefly into the parameters of the Hubbard model [Eq. (1)]. These can be determined from the microscopic quantities such as the potential depths $V_{F(B)}$ due to the laser seen by the atoms and their recoil energies $E_{F(B)}^R$ $=\hbar^2 k_L^2/2m_{F(B)}$, where k_L is the wave vector of the laser and $m_{F(B)}$ are the masses of the fermions (bosons). The potential depth seen by the atoms depend on the detuning of the laser from their natural wavelengths $\lambda_{F(B)}$ of the fermions (bosons). In fact, it can be shown that the ratio of the lattice potentials seen by the fermions and bosons are [21]

$$\frac{V_F}{V_B} = \frac{\lambda_F^4 \Gamma_F \Delta\lambda_B}{\lambda_B^4 \Gamma_B \Delta\lambda_F}, \qquad (5)$$

where $\Delta\lambda_{F(B)} = \lambda_L - \lambda_{F(B)}$ denote the detunings for the fermions (bosons) and $\Gamma_{F(B)}$ are the corresponding natural linewidths. Since the ratio of the natural linewidths is generally close to unity [14,21], we see that one can tune the ratio of the lattice depths seen by bosons and fermions by varying the detunings.

In terms of these quantities, we have [17]

$$t_{B(F)} = (2/\sqrt{\pi})(E_{B(F)}^R V_{B(F)}^3)^{1/4} e^{-2\sqrt{V_{B(F)}/E_{B(F)}^R}},$$

$$U_{BB(FF)} = \sqrt{8/\pi}(E_{B(F)}^R V_{B(F)}^3)^{1/4} k_L a_{BB(FF)},$$

$$U_{FB} = \frac{(E_F^R V_B^3 V_F^3)^{1/4}(1 + m_F/m_B) k_L a_{BF}}{\sqrt{\pi/16}(\sqrt{V_B} + \sqrt{V_F E_B/E_F})^{3/2}}, \qquad (6)$$

where a_{FF}, a_{BB}, and a_{FB} are the s-wave scattering lengths for interaction between two fermions, two bosons, and a fermion and a boson, respectively. These scattering lengths also can be varied either by choosing different species of fermions or bosons or by tuning them using Feshbach resonance. Further, as we have discussed before, by choosing the laser detuning we can also make the fermions and bosons see either similar or very different lattice potentials. Therefore, instead of calculating these parameters from the microscopics, we shall aim to portray a general picture of the Mott phase diagram. Since the experimental possibilities are limitless, for the sake of brevity, we choose $U_{BB}=U_{FF}=U$ and vary the ratios λ $=U_{BF}/U$ and $\eta=t_F/t_B$. It is clear from the above discussions that such a situation can be always achieved in experiments. We shall consider some such specific examples in Sec. IV.

Next, we consider the Bose-Fermi Hubbard Hamiltonian in the Mott limit. In this limit, the on-site states can be represented as $|n_0^B, n_0^F\rangle$ and the energy is given by

$$E[n_0^B, n_0^F] = E_F[n_0^F] + E_B[n_0^B] + E_{FB}[n_0^B, n_0^F],$$

$$E_F[n_0^F] = -\left(\mu_F' - \frac{1}{2}\right)n_0^F + \frac{1}{2}(n_0^F - 1)^2,$$

$$E_B[n_0^B] = -\mu_B' n_0^B + \frac{1}{2}n_0^B(n_0^B - 1),$$

$$E_{FB}[n_0^B, n_0^F] = \lambda n_0^F n_0^B, \qquad (7)$$

where we have scaled all energies by U and $\mu_{F(B)}'$ $=\mu_{F(B)}/U$. It can be seen from Eqs. (7) that two states $|n_0^B, n_0^F - 1\rangle$ and $|n_0^B - 1, n_0^F\rangle$ are degenerate when

$$(\lambda - 1)(n_0^F - n_0^B) = \mu_F - \mu_B, \qquad (8)$$

whereas three states $|n_0^B, n_0^F\rangle$, $|n_0^B, n_0^F - 1\rangle$, and $|n_0^B - 1, n_0^F\rangle$ are degenerate when

$$\mu_F' = (n_0^F + n_0^B \lambda - 1),$$

$$\mu_B' = (n_0^F \lambda + n_0^B - 1). \qquad (9)$$

The conditions of these degeneracies, of course, depend on our choice of parameters of the model. It is also to be noted that in Eqs. (8) and (9), n_0^F and n_0^B in the ground state are themselves functions of μ_F', μ_B', and λ, and have to be determined by minimizing Eq. (7) subject to the constraint of n_0^F and n_0^B being integers.

The ground state phase in the Mott limit ($t_b=t_F=0$) diagram can be obtained by numerically minimizing the ground state energy [Eq. (7)] for integers $0 \le n_0^F \le 2$ and n_0^B. For the sake of brevity, we carry out the numerical computation for
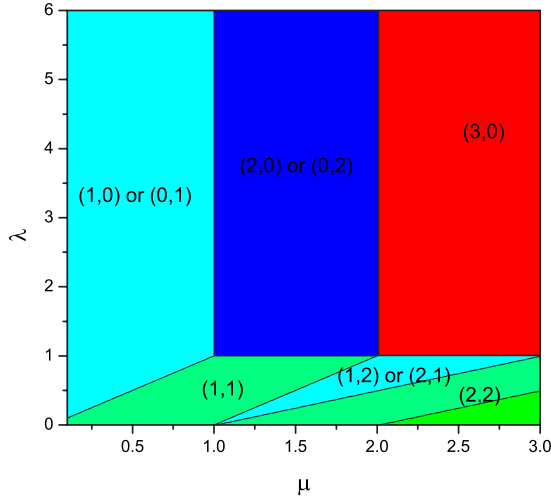
FIG. 1. (Color online) Ground state phase diagram in the atomic limit for $\mu = \mu'_B = \mu'_F$ and $\lambda > 0$. The phases are marked by values of (n_0^B, n_0^F) in the ground state. For large λ, the system tries to avoid putting bosons and fermions at the same site. The threefold degeneracy between $(1,0)$ and $(0,1)$ as well as $(2,1)$ and $(1,2)$ occur for a large portion of the phase diagram. In addition, there are doubly degenerate regions such as $(2,0)$ and $(0,2)$. These degeneracies are lifted by the virtual hopping process for small but finite t_B and t_F.

$\mu'_B = \mu'_F = \mu$ and present the phase diagram as a function of μ and λ. The phase diagram for $\lambda > 0$ is shown in Fig. 1. We find, as expected from the results of Ref. [21], for $\lambda > 1$, the fermions and the bosons repel each other out from a given site so that a site is occupied by either a boson or a fermion, but not both. Such states were dubbed as "composite" states of bosons and fermions with a correlation hole of fermions and bosons in Ref. [21]. However, in the present scenario, the spins of the fermions are dynamical degrees of freedom which lead to richer variety of possible phases, as we discuss below.

As expected from discussions leading to Eq. (8), a large portion of the phase diagram has degenerate ground states corresponding to $|n_0^B = 0, n_0^F = 1\rangle$ and $|n_0^B = 1, n_0^F = 0\rangle$. Note that in terms of the original fermions, the degeneracy is actually threefold corresponding to states $|0, \uparrow\rangle$, $|0, \downarrow\rangle$, and $|1, 0\rangle$. This degeneracy is lifted by quantum fluctuations due to the presence of small but finite t_F and t_B. This can lead to three different ground states as sketched in Fig. 2: (A) an antiferromagnetic state of fermions with no bosons, (B) a state of one boson per site and no fermions, and (C) a state with fermions and bosons being the nearest neighbors with an antiferromagnetic order for the fermions. The energies of these states can be estimated using a straightforward $O(t_{B(F)}^2/U^2)$ perturbation theory and are given by

$$E_A = -\frac{Nzt_F^2}{U} = -\frac{Nzt_B^2}{U}\eta^2,$$

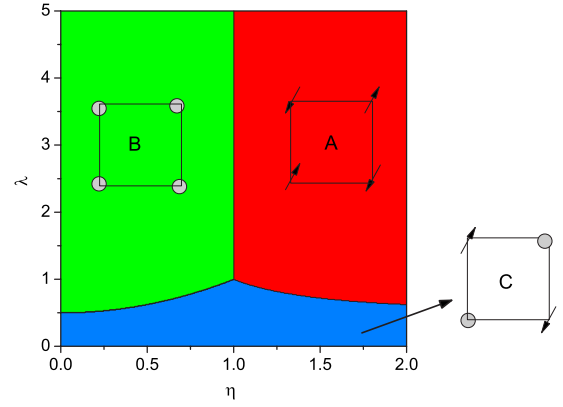$$E_B = -\frac{2Nzt_B^2}{U},$$

FIG. 2. (Color online) Possible ground states A, B, and C that result from lifting the classical degeneracy of the ground states $(n_0^B, n_0^F) = (1,0)$ and $(0,1)$ due to quantum fluctuations. Notice that the antiferromagnetic ordering of state C is different from state A and is a consequence of very weak next-nearest-neighbor hopping. Similar states will result when the degeneracy of the states $(2,1)$ and $(1,2)$ is lifted.

$$E_C = -\frac{Nzt_B^2}{2\lambda U}(1 + \eta^2), \qquad (10)$$

where N is the total number of sites in the system and z is the coordination number of each site. Comparing the energies of the states from Eq. (10), we find that state A is favored over B and C when $\eta^2 > 2$ and $\lambda > (1 + \eta^{-2})/2$. Similarly the state B is favored for $\eta^2 < 2$ and $\lambda > (1 + \eta^2)/4$ and state C for small λ when $(1 + \eta^2)/(2\lambda) > \max[2, \eta^2]$. The corresponding phase diagram is shown in Fig. 2.

With only a nearest-hopping term in the Hamiltonian, the antiferromagnetic ordering in the ground state C is in fact frustrated. Indeed, fourth-order (in t) virtual hopping leads to an antiferromagnetic coupling both between next-nearest-neighbor sites and next-next-nearest sites (Fig. 3). In practice, however, this frustration is suppressed by $O(t'^2/U)$ cor-
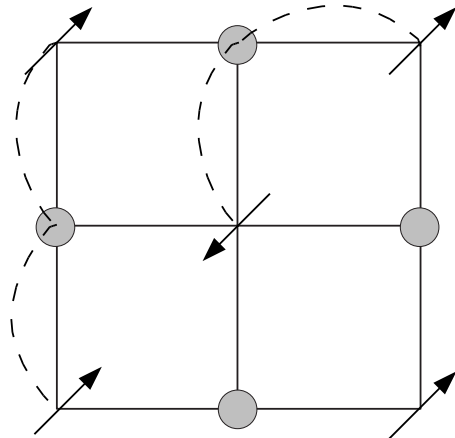

FIG. 3. Virtual hopping (dashed lines) leading to frustration of the antiferromagnetic ground state C. This frustration is lifted and an antiferromagnetic ground state stabilized by virtual hopping generated by the kinetic coupling t' between next-nearest-neighbor sites (located at opposite corners of the square lattice unit cell).
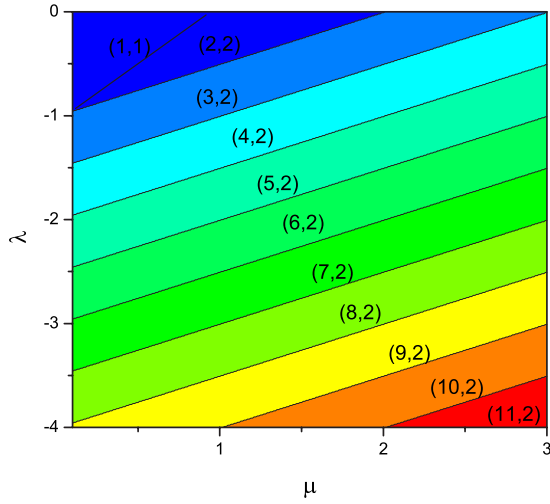
FIG. 4. (Color online) Ground state phase diagram in the Mott limit for $\lambda < 0$. The number of fermions per site is $n_0^F = 2$ while the number of bosons per site is shown in each phase for large negative λ.

rections that arise from the next-nearest-neighbor hopping t' [not included in the Hamiltonian (2)], leading to an antiferromagnetic order at wave vector $(\pi/a, 0)$ [or $(\pi/\sqrt{2}a, \pi/\sqrt{2}a)$ in a reference frame tilted by 45°], in two dimensions as shown in Fig. 2. This should be contrasted with the usual $(\pi/a, \pi/a)$ ordering realized either for state A or for the (1,1) state shown in Fig. 1. Additional hopping amplitudes (e.g., the next-next-nearest-neighbor hopping t'') are expected to be smaller and will not affect the antiferromagnetic ordering of the ground state C. A similar consideration applies for the degenerate states (2,1) and (1,2) where quantum fluctuations will similarly lift the degeneracies. Notice that the possibilities of having a ferromagnetic state of fermions where all sites are uniformly occupied by $\uparrow$ or $\downarrow$ fermions never occur since such a state necessarily suppresses fermion hopping due to the Pauli principle and is thus higher in energy compared to the state A.

Finally, we point out that lifting of degeneracy by quantum fluctuations also occurs for the twofold degenerate states labeled as (2,0) or (0,2). Note that the state (2,0) corresponding to two fermions per site requires that all second order virtual hopping processes are suppressed, unless higher bands are involved. Hence such a state is energetically unfavorable and is never realized. The two other states are (D) a homogeneous state with two bosons per site and (E) a state with alternate arrangements of two bosons and two fermions per site. The energies of these states are given by $E_D = -6Nzt_B^2/U$ and $E_E = -Nzt_B^2(1+\eta^2)/(2\lambda-1)U$. The latter state E is thus favored over state D for $\eta^2 > 6(2\lambda-1)-1$.

In contrast for $\lambda < 0$ (i.e., $U_{BF} < 0$), there are no degeneracies. The (1,1) state persists at small negative λ. For $|\lambda| > 1$, the system always has two fermions per site with n_0 bosons, where n_0 is the integer which minimizes $E[n_0] = -\mu n_0 + n_0(n_0-1)/2 - 2|\lambda|n_0$. The phase diagram is shown in Fig. 4 as a function of μ and λ. The phase diagram corresponds to the Mott phase of bosons coupled with nondynamical fixed number of fermions. Note that analogous com-

posite states with n_0 bosons and one fermion were found and dubbed as "composite fermion" states in Ref. [21]. Here we have almost identical states at large negative λ with the difference that there are two fermions per site (instead of one per site as in Ref. [21]) owing to the fact that fermion spins are not frozen in the present study.

III. SLAVE-ROTOR MEAN-FIELD THEORY

In this section, we construct a slave-rotor mean-field theory for the coupled Bose-Fermi problem and use it to study the metal–superfluid-insulator transition in this system. We develop the formalism for the mean-field theory in Sec. III A, and discuss the results obtained in Sec. III B.

A. Formalism

We begin by implementing the slave-rotor formalism [24] in the present context. This key observation behind this formalism is that the fermionic Hubbard Hamiltonian [Eq. (2)] can be mapped onto a Hamiltonian of free auxiliary fermions coupled self-consistently to a quantum rotor. The chief advantage of this representation is that the quartic interaction term of the original fermionic Hubbard model can now be represented by a quadratic term in the rotor variables and can thus be treated exactly in the Mott limit. This feature makes this technique suitable for studying Hubbard models in the strong-coupling regime. Further, as shown in Ref. [24], the metal-insulator transition of the original fermions can be looked upon as the order-disorder transition of the rotors which facilitates the study of metal-insulator transition.

To begin with, we note the identity

$$\frac{1}{2}\left[\sum_\sigma \left(n_{i\sigma}^F - \frac{1}{2}\right)\right]^2 = n_{i\uparrow}^F n_{i\downarrow}^F - \frac{1}{2}\sum_\sigma n_{i\sigma}^F + \frac{1}{2} \quad (11)$$

so that, up to a constant term, one can write Eq. (2) as

$$\mathcal{H}_F = -t_F \sum_{\langle ij \rangle \sigma} (c_{i\sigma}^\dagger c_{j\sigma} + \text{H.c.}) - \left(\mu_F - \frac{U}{2}\right)\sum_{i\sigma} n_{i\sigma}^F$$
$$+ \frac{U}{2}\sum_i \left[\sum_\sigma \left(n_{i\sigma}^F - \frac{1}{2}\right)\right]^2. \quad (12)$$

Next, following Ref. [24], we introduce the slave-rotor representation for the fermions. The key observation here is that the spectrum of H_F in the Mott limit depends only on the total fermion number $\sum_\sigma n_{i\sigma}$ which can be represented by eigenvalues of angular momenta of an $O(2)$ rotor. Thus we write the physical fermion annihilation operator as

$$c_{i\sigma} = f_{i\sigma}\exp(-i\theta_i), \quad (13)$$

where $f_{i\sigma}$ denotes the annihilation operator for the pseudofermion and θ_i denotes the rotor variable at site i. The corresponding angular momentum of the rotor is denoted by $L_i = -i\partial_{\theta_i}$. In this representation, a physical fermion state can be written as a product of the pseudofermion state and a rotor state as

$$|c_1, c_2, \ldots, c_Q\rangle_i = |f_1, f_2, \ldots, f_Q\rangle_i |l = Q - 1\rangle_{\theta_i}. \tag{14}$$

Here l denotes the eigenvalues of the rotor angular momentum L and $|c_1, c_2, \ldots, c_Q\rangle$ is the antisymmetric combination of fermionic states for $Q = l + 1$ fermions at site i. Note that whereas for ordinary rotors l can take all possible integer values, here it is constrained to range between -1 and 1 by the operator identity

$$L_i = \sum_\sigma \left(f_{i\sigma}^\dagger f_{i\sigma} - \frac{1}{2} \right). \tag{15}$$

With the following constraint, one can write Eqs. (12) and (4) in terms of the rotor variables as

$$\mathcal{H}_F = -t_F \sum_{\langle ij \rangle \sigma} (f_{i\sigma}^\dagger f_{j\sigma} \exp[i(\theta_i - \theta_j)] + \text{H.c.})$$
$$- \left(\mu_F - \frac{U}{2} \right) \sum_{i\sigma} f_{i\sigma}^\dagger f_{i\sigma} + \frac{U}{2} \sum_i L_i^2, \tag{16}$$

$$\mathcal{H}_{FB} = \lambda U \sum_{i\sigma} f_{i\sigma}^\dagger f_{i\sigma} n_i^B. \tag{17}$$

with L_i related to $\sum_\sigma f_{i\sigma}^\dagger f_{i\sigma}$ by Eq. (15). In the Mott limit ($t_F = t_B = 0$), we can implement the constraint [Eq. (15)] exactly and this procedure leads to Eq. (7) with $n_0^F = Q = l + 1$ in a straightforward manner. Note also that the quartic interaction term $U \sum_i n_{i\uparrow} n_{i\downarrow}$ in Eq. (2) has now been replaced by a quadratic term $U \sum_i L_i^2 / 2$ in Eq. (16). This has been done at the expense of generating a nonlinear coupling between the auxiliary fermions and the rotors, as is evident from the first term of Eq. (16).

When $t_F, t_B \neq 0$, the abovementioned constraint condition cannot be implemented exactly and we need to resort to mean-field approximation. The slave-rotor mean-field theory for the present system can be developed by a straightforward generalization of the formalism developed in Ref. [24]. To begin with, we write the system Hamiltonian $\mathcal{H}$ as

$$\mathcal{H} = H_r + H_f + H_b, \tag{18}$$

$$H_r = -\sum_{\langle ij \rangle} \tau_{ij}^{\text{eff}} \cos(\theta_i - \theta_j) + \sum_i \frac{U}{2} L_i^2 + h L_i, \tag{19}$$

$$H_f = -\sum_{\langle ij \rangle, \sigma} (t_{ij}^{\text{eff}} f_{i\sigma}^\dagger f_{j\sigma} + \text{H.c.})$$
$$+ \sum_{i\sigma} (-\mu_F + U/2 + h + \lambda U \bar{n}_B) f_{i\sigma}^\dagger f_{i\sigma}, \tag{20}$$

$$H_b = -t_b \sum_{\langle ij \rangle} (b_i^\dagger b_j + \text{H.c.})$$
$$+ \frac{U}{2} \sum_i n_i^B (n_i^B - 1) - (\mu_b - \lambda U \bar{n}_F) \sum_i n_i^B, \tag{21}$$

where we have implemented the constraint (15) using an auxiliary field h_i which has been replaced by its saddle point value h at the mean-field level. Here we also treat the coupling between the bosons and the fermions within mean-field

approximation by replacing the fermion and boson density operators $n_i^{B/F}$ by their averages $\bar{n}_{B/F}$. This amounts to replacing the term $\Sigma_i \lambda U n_i^F n_i^B$ by $\Sigma_i \lambda U n_i^F \bar{n}_B$ in Eq. (20), and by $\Sigma_i \lambda U n_i^B \bar{n}_F$ in Eq. (21). Within this mean-field approximation, the coupling term acts as a density-dependent shift in the chemical potentials for the bosons and the fermions. The effective hopping matrix elements t_{ij}^{eff} and τ_{ij}^{eff} in Eqs. (19) and (20) are given by

$$t_{ij}^{\text{eff}} = t_{ij} \langle \cos(\theta_i - \theta_j) \rangle_{H_r},$$
$$\tau_{ij}^{\text{eff}} = t_{ij} \left\langle \sum_\sigma f_{i\sigma}^\dagger f_{j\sigma} \right\rangle_{H_f}, \tag{22}$$

with the assumption that averages such as $\langle \exp(\theta_i - \theta_j) \rangle$ and $\langle \Sigma_\sigma f_{i\sigma}^\dagger f_{j\sigma} \rangle$ are real on each bond [24].

The next step is to approximate the rotor model by an effective single site model

$$H_r' = \sum_i \left(K \cos(\theta_i) + \frac{U}{2} L_i^2 + h L_i \right), \tag{23}$$

$$K = -2 \sum_j \tau_{ij}^{\text{eff}} \langle \cos(\theta_j) \rangle_{H_r}. \tag{24}$$

Note that this approximation makes sense only when the Mott ground state does not have density wave order of any kind either for bosons or fermions. Using the fact that under this approximation the H_r' becomes a single site Hamiltonian, we define

$$Z = \langle \cos(\theta) \rangle_{H_r}^2 \tag{25}$$

and use H_f to compute all averages involving the fermionic fields. This yields

$$K = 4 \langle \cos(\theta) \rangle_{H_r} \int d\epsilon \, \epsilon n_F (Z\epsilon - \mu_F + h + \lambda U \bar{n}_B)$$
$$= 4 \langle \cos(\theta) \rangle_{H_r} \bar{\epsilon}, \tag{26}$$

$$\langle L \rangle = 2 \left[\int d\epsilon D(\epsilon) \theta (Z\epsilon - \mu_F + U/2 + h + \lambda U \bar{n}_B) \right] - 1$$
$$= 2\bar{n}_F - 1, \tag{27}$$

where the density of states $D(\epsilon)$ is defined as $D(\epsilon) = \int d^3 k \, \delta(\epsilon - \epsilon_k) / (2\pi)^3$, and $\epsilon_k = -2t \Sigma_{i=x,y,z} \cos(k_i)$ is the kinetic energy of the fermions (all momenta are measured in units of lattice spacing), and $\bar{\epsilon}$ and $\bar{n}_F$ are the average fermionic kinetic energy and density, respectively. Comparing the expression of $\bar{n}_F$ with that for the free fermions $\bar{n}_F = \int_\infty^{\mu_0} D(\epsilon) d\epsilon$, where μ_0 is the chemical potential for the free fermions at $T = 0$, one has the relation

$$Z\mu_0 = \mu_F - U/2 - h - \lambda U \bar{n}_B, \tag{28}$$

$$\langle L \rangle = 2\bar{n}_F - 1. \tag{29}$$

Notice that since Z vanishes at the transition at $\mu_F = \mu_F^c$, one gets $\mu_F^c - U/2 = h + \lambda U \bar{n}_B$. Thus Z acts as the order parameter

for the metal-insulator transition of the fermions.

Equations (25)–(29) have to be self-consistently solved to obtain the ground state of the system. However, to do this, one needs to obtain the ground state of the bosonic Hamiltonian [Eq. (21)] and compute the average value of the boson density $\bar{n}_B$. Since at the mean-field level, the average fermionic density $\bar{n}_F$ enters the boson Hamiltonian as a shift in the chemical potential, one can use the projection operator technique developed in Ref. [11] for obtaining $\bar{n}_B$. It was shown in the context of two-species bosons that the projection operator method compares well with quantum Monte Carlo results [11].

The projection operators for the boson Hamiltonian [Eq. (21)] can be constructed following the procedure of Ref. [11]. It is given by

$$P_l = (|n_0^B\rangle_i \langle n_0^B|_i) \otimes (|n_0^B\rangle_j \langle n_0^B|_j), \qquad (30)$$

where n_0^B is the boson occupation per site for the Mott ground state and l denotes the link connecting two neighboring sites i and j.

The hopping term for the bosons can be rewritten in terms of the sum over links as

$$T = \sum_l T_l = -t_b \sum_l (b_i^\dagger b_j + \text{H.c.}), \qquad (31)$$

where i and j are near neighbor sites connecting the link l. In this notation, one can now divide the hopping terms into two parts

$$T_l = T_l^1 + T_l^0 = (P_l T_l + T_l P_l) + P_l^\perp T_l P_l^\perp, \qquad (32)$$

where $P_l^\perp = 1 - P_l$. It is then easy to see that the term $T^1 = \sum_l T_l^1$ acting on the ground state takes one out of the ground state manifold. The idea is therefore to seek a canonical transformation operator S which eliminates T_1 to $O(t_B/U)$ from the low-energy effective Hamiltonian $[iS, H_0] = -T^1$, where H_0 denotes all the on-site terms in Eq. (4). The effective low-energy Hamiltonian can be obtained by the usual Schrieffer-Wolff transformation method

$$H^* = \exp(iS) H \exp(-iS) \qquad (33)$$

$$= H_0 + T^0 + [iS, T] + \frac{1}{2}[iS, [iS, H_0]] + \cdots. \qquad (34)$$

Note that this is equivalent to a systematic t_B/U expansion and all the omitted terms denoted by ellipsis are at least $O(t_B^3/U^3)$.

The next task is to find out the canonical transformation operator S in terms of the projection operators P_l. Following Ref. [11], we guess the form of the S to be

$$S = i\alpha \sum_l [P_l, T_l], \qquad (35)$$

where the coefficient α is to be determined by the condition $[iS, H_0] = -T^1$. To do this we use the operator identities

$$[P_l T_l, H_0] = U P_l T_l, \quad [T_l P_l, H_0] = -U T_l P_l \qquad (36)$$

and evaluate $[iS, H_0]$ to be

$$[iS, H_0] = -\frac{\alpha}{U} \sum_l (P_l T_l + T_l P_l) = -T^1 \frac{\alpha}{U}. \qquad (37)$$

Thus we find that setting $\alpha = U$ we obtain the expression for $S = i\sum_l [P_l, T_l]/U$, which eliminates T_1 to $O(t_B/U)$ from the low-energy effective Hamiltonian.

The effective Hamiltonian can be now rewritten by substituting the condition $[iS, H_0] = -T^1$ in the last term of Eq. (34) as

$$H^* = H_0 + T^0 - \sum_{l,l'} [[P_l, T_l], T_{l'}^0 + T_{l'}^1/2]. \qquad (38)$$

With some algebra we now reach the final form of the low energy effective boson Hamiltonian which takes into account all t_B^2/U^2 fluctuations

$$H^* = H_0 + T^0 - \frac{1}{U}\left[\sum_l (P_l T_l^2 P_l - T_l P_l T_l) \right.$$
$$\left. + \sum_{l,l'} \left\{ P_l T_l T_{l'} - T_l P_l T_{l'} - \frac{1}{2}(P_l T_l T_{l'} P_{l'} - T_l P_l P_{l'} T_{l'}) \right\} \right], \qquad (39)$$

where l and l' are nearest neighbor links. One can now use an on-site variational wave function in the same way as in Ref. [11]

$$\Psi_v = \prod_i (a|n_0^B\rangle_i + b|n_0^B + 1\rangle_i + c|n_0^B - 1\rangle_i) \qquad (40)$$

to minimize the ground-state energy $E_G = \langle \Psi_v | H^* | \Psi_v \rangle$ and obtain the corresponding boson density $\bar{n}_B$ and superfluid order parameter Δ

$$\bar{n}_B = |a_G|^2 n_0^B + |b_G|^2 (n_0^B + 1) + |c_G|^2 (n_0^B - 1), \qquad (41)$$

$$\Delta = \sqrt{n_0^B + 1} a_G^* b_G + \sqrt{n_0^B} c_G^* a_G, \qquad (42)$$

where a_G, b_G, and c_G are values of the coefficients a, b, and c in the variational ground state. A comparison of the phase diagram obtained by minimizing $E_v = \langle \Psi_v | H^* | \Psi_v \rangle$ for $\lambda = 0$ with analogous phase diagrams obtained from mean-field theory [3,5,6] and defect phase calculations to $O(t_B^2/U^2)$ [26] is presented in the Appendix.

Equations (41) and (42) combined with Eqs. (25)–(29) can now be solved self-consistently to obtain a mean-field description of the coupled Fermi-Bose system near the metal–superfluid-insulator transition points which are signaled by the onset of a nonzero Z or Δ. This method, therefore, allows for a self-consistent treatment for the coupled Bose-Fermi problem near the metal–superfluid-insulator transition point, provided that the insulating ground state preserves translational symmetry.
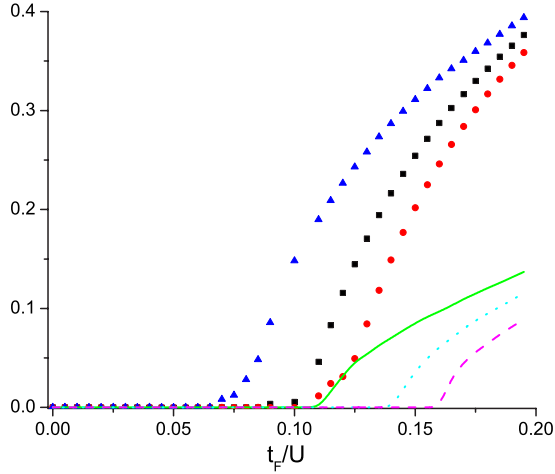
FIG. 5. (Color online) Plot of the order parameter Δ and Z for $\mu/U=0.7$ and $\eta=5$. Nonzero values of Δ/Z signals superfluid–metal-insulator transition for the bosons and fermions. The symbols are as follows: black squares and green solid line (Δ and Z, respectively, for $\lambda=0$), red circles and cyan dotted line (Δ and Z, respectively, for $\lambda=0.3$), and blue triangles and magenta dashed line (Δ and Z, respectively, for $\lambda=0.5$).

B. Results

In this section, we discuss the results of application of the formalism developed in the last section to the problem at hand. Here we shall concentrate on the (1,1) Mott state for the following reasons. First, since we would be interested in studying metal-insulator transitions for fermions together with the superfluid-insulator transition of bosons, we would like to concentrate on Mott states which have one fermion per site. Second, in the formalism developed in Sec. III A, we treat the Bose-Fermi interaction term within mean-field approximation, we would like to restrict ourselves to the parameter regime $|\lambda|=|U_{FB}/U|<1$, where the mean-field results are expected to be more accurate.

To demonstrate the effect of interspecies interaction, we first concentrate on a fixed value of $\mu_F=\mu_B=0.7U$ and $\eta=t_F/t_B=5$, and study the onset of metal–superfluid-insulator transition as a function of t_F/U for a few representative values of λ. A plot of Z and Δ for this case is shown in Fig. 5 while the fermionic and bosonic densities are plotted in Fig. 6. The results of these plots can be understood as following. Consider fixing η and gradually increasing t_F so that the fermions and bosons move towards a metal–superfluid-insulator transition point. As long as the bosons and fermions are in the Mott state, their densities are pinned to $n_0^B=1$ or $n_0^F=1$, and hence the fermions and bosons see a fixed chemical potential $\mu_{F(B)}^{\text{eff}}=\mu-\lambda U n_0^{B}(n_0^F)$. For our chosen value of η, the metal-insulator transition occurs before the superfluid-insulator transition of the bosons at $t_F^c(\lambda)=t_F^c(\mu_F^{\text{eff}})$. Notice that $t_F^c(\lambda)$ is a nonmonotonic function of λ for a given μ and η. Hence the metal-insulator transition for the fermions can either be enhanced ($\lambda=0.5$) or hindered ($\lambda=0.1$) due to the Bose-Fermi interaction. Once the fermions have delocalized, the density of fermions changes with t_F for a fixed chemical potential μ as seen in Fig. 6. Hence the effective chemical
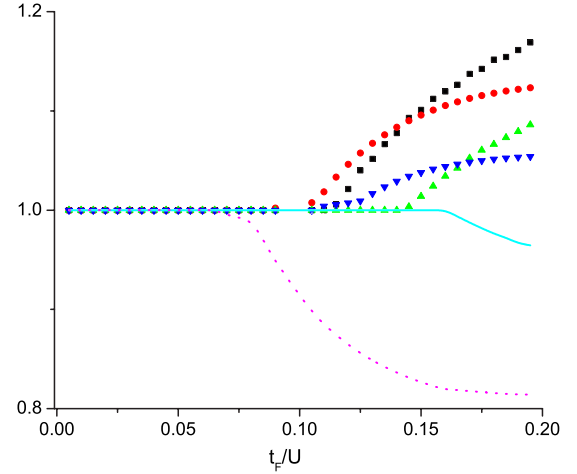

FIG. 6. (Color online) Plot of the average densities $\bar{n}_B$ and $\bar{n}_F$ for the bosons and fermions for $\mu/U=0.7$ and $\eta=5$. The deviation of the densities from their quantized values in the Mott state signals the onset of metal-insulator transition for fermions and superfluid-insulator transition for the bosons. The symbols are as follows: black squares and red circles ($\bar{n}_B$ and $\bar{n}_F$, respectively, for $\lambda=0$), green up triangles and blue down triangles ($\bar{n}_B$ and $\bar{n}_F$, respectively, for $\lambda=0.3$), magenta dotted line and cyan solid line ($\bar{n}_B$ and $\bar{n}_F$, respectively, for $\lambda=0.5$).

potential seen by the bosons now becomes a function of both $t_B=t_F/\eta$ and λ. Thus by increasing t_B, we actually traverse a curve with a finite slope in the μ-t_B plane in contrast to the noninteracting ($\lambda=0$) case. Consequently, the superfluid-insulator transition of the bosons occurs at $t_B^c(\lambda)$ which can be quite different from $t_B^c(\lambda=0)$. We note this effect may lead to both enhancement $[t_B^c(\lambda)>t_B^c(\lambda=0)]$ or hindrance $[t_B^c(\lambda)<t_B^c(\lambda=0)]$ of the superfluid-insulator transition of the bosons depending on the chosen values of η and μ, as can be seen by comparing Figs. 5 and 7. For the choice of $\mu/U=0.7$ and $\eta=5$, we find that $t_B^c(\lambda)>t_B^c(\lambda=0)$, whereas the reverse case is realized for $\mu/U=0.4$ and $\eta=4$. In the latter
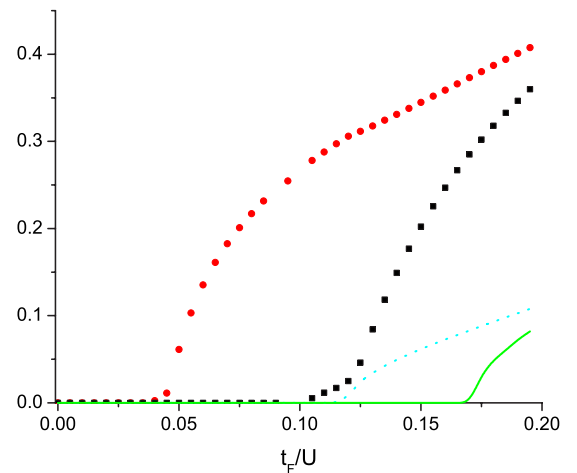

FIG. 7. (Color online) Plot of Δ and Z for $\mu/U=0.4$, $\eta=4$ and $\lambda=0$ and $\lambda=0.3$. All symbols have the same meaning as Fig. 5. The plot serves as an illustration that repulsive interaction between bosons and fermions can enhance metal-superfluid transitions.
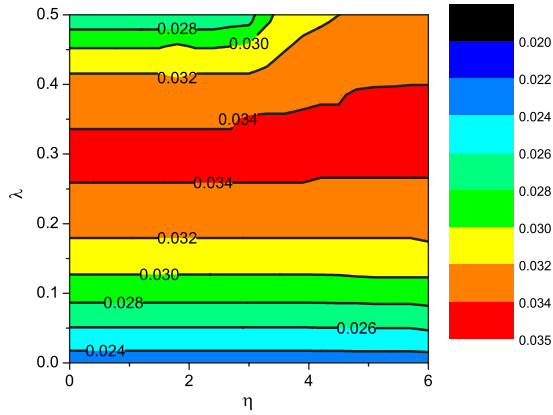
FIG. 8. (Color online) Plot of t_B^c/U as a function of η and λ for $\mu/U=0.7$. For small η, the fermions remain in the Mott state when the superfluid-insulator transition of the bosons takes place whereas for large η they have already undergone a metal-insulator transition.

case, both the metal-insulator transition for the fermions and the superfluid-insulator transition for the bosons are enhanced for $\lambda>0$. Hence we conclude that a repulsive Bose-Fermi interaction can either enhance or hinder the onset of metal–superfluid-insulator transition of a coupled Bose-Fermi mixture held at a fixed chemical potential. Notice that this effect is absent if the boson and the fermion densities are held constant individually, since in that case, there is no influence of the fermionic metal-insulator transition on the bosonic superfluid-insulator transition within the mean-field theory. This is of course an artifact of the present mean-field approximation. Clearly, the dynamics of the fermions and bosons should play an important role in the transition. For example, near the metal insulator of the fermions, there will be density fluctuations which give the bosons a chance to hop to a neighboring site even if they would remain localized in the absence of such fluctuations. A treatment of this effect requires analysis of the slave-rotor model beyond the present mean-field approximation and is outside the scope of the present study.

Finally, we present a plot of the critical hopping strength t_B^c in Fig. 8 as a function of η and λ for a fixed representative $\mu/U=0.7$. We note that at small η, the superfluid-insulator transition takes place when the fermions are still in the Mott state with their density pinned at $n_F^0=1$. Consequently, the transition for the boson, within the simple mean-field theory, is the same as that occurring for $\mu_{\text{eff}}=\mu-\lambda U$; t_B^c becomes maximum when $\mu_{\text{eff}}/U \approx 0.4$ or $\lambda \approx 0.3$. However, when η is large, the fermions have already undergone the metal-insulator transition when the bosons are at their transition point and hence have $\langle n_F\rangle \neq 1$. Consequently the bosons see a different $\mu_{\text{eff}}=\mu-\lambda U\langle n_F\rangle$ and hence the value of t_B^c changes. This is reflected in bending of the phase boundary in the right half of Fig. 8. Analogous plots for t_F^c will have qualitatively same features.

Before closing this section we would like to make a few qualitative comments. First, the analysis of the phase diagram for negative λ with $|\lambda|\lesssim 1$ can be carried out in a similar manner and one obtains qualitatively similar results in this case. Second, at large and negative λ, the Mott states

correspond to two fermions and $n_0(\lambda)$ bosons localized per site. In this case, with decreasing lattice potential, the bosons would undergo a superfluid-insulator transition with the fermions still in the Mott phase. Therefore the superfluid-insulator transition of the bosons can be described, within mean-field theory, by a Hubbard model of bosons with effective chemical potential $\mu_{\text{eff}}=\mu-2\lambda U$. As we decrease the lattice depth, the fermions would eventually delocalize when the hopping coefficient t_F becomes comparable to the energy gap between the single particle levels $(E_n \simeq 5E_R)$ in the potential wells. However, this is a large energy scale $(E_n \gg U, \lambda U)$ for deep lattices and so for any reasonable value of η, one expects the superfluid-insulator transition of bosons to occur while the fermions are still in the Mott state. Third, we would like to note that the slave-rotor mean-field theory worked out here cannot be applied for states with broken translational symmetries in terms of boson and fermion numbers (such as the state C shown in Fig. 2) since we have used a single-site approximation for the slave-rotor mean-field theory. Also the present slave-rotor treatment is expected to be more inaccurate for states with $\lambda \gg 1$ since the fermion-boson interaction is treated at a mean-field level within our scheme. Nevertheless we note that qualitatively we would expect a Mott-superfluid–metal transition from these phases as λ is reduced keeping the density of bosons and fermions constant. Finally, the present theory cannot address the question of possible superconducting instability of the fermions in the metallic state. This issue is discussed in Ref. [21]. A generalization of our mean-field description of the superfluid–metal-insulator transitions to address such issues and inclusion of the effect of quantum fluctuations beyond the mean-field treatment used here remain open problems to be addressed in future work.

IV. EXPERIMENTS

A large part of the Mott phases and the superfluid-insulator transition of the Bose-Fermi mixtures discussed here can be experimentally accessed using standard experiments on specific Bose-Fermi mixtures. Before going into details of specific systems, let us first outline some typical experiments that can be performed on these systems. One such experiment that is routinely carried out in atomic systems is measurement of momentum distribution of atoms in the trap [1]. This is typically done in a time of flight measurement by letting the atoms fly out by dropping both the lattice and the trap and then measuring the position distribution of the expanding atom cloud. Such a position distribution measurement yields information about momentum distribution of the atoms within the trap. These experiments obtain qualitatively different signatures for atoms in the Mott and the superfluid states for bosons [1,2], but cannot distinguish between the Bose and the Fermi atoms. To achieve this distinction, one needs to pass the expanding atom cloud through a Stern-Gerlach apparatus. Since the fermions and the bosons have different spins (or total angular momenta), they will get separated during this process and can thus be distinguished. Such Stern-Gerlach experiments have been carried out with bosonic atoms in Refs. [27,28] and their

generalization to present systems should be straightforward. Finally, the antiferromagnetic order of fermions in the Mott phases [either the (1,1) phase in Fig. 1 or the phases A and C shown in Fig. 2] can be determined by measuring spatial noise correlations of the expanding cloud in a time of flight measurement [29,30].

Let us now consider some specific Bose-Fermi mixtures that have been realized experimentally. One such system is ^{6}Li and ^{7}Li mixtures with $a_{FF}=a_{BB}=5a_0$ and $a_{BF}>0$ [31,32], where a_0 is the Bohr radius. The value of a_{BF} has not been unambiguously measured in this system, but is expected to be positive indicating a repulsive interaction [31]. For this mixture, $m_F \simeq m_B$ and depending on the value of a_{BF} and by varying the frequencies of the laser providing the optical lattice (as discussed in Sec. II), we may realize different points on the phase diagram shown in Fig. 1. Of particular interest is the case where $a_{BF}>a_{FF}$ [21]. In this case, for one atom per site, we expect to obtain one of the Mott phases A, B, or C shown in Fig. 2 depending on the specific value of $\lambda \sim a_{BF}/a_{FF}$ and $\eta=t_B/t_F$ which can be varied by slightly changing the ratio V_F/V_B [Eq. (6)] [33]. In this case, one can scan a large part of the phase diagram shown in Fig. 2. The possible antiferromagnetic orders of fermions in phase A or C (Fig. 2) can be determined by measuring the spatial noise correlation measurements [29]. The states B and C can also be distinguished by passing the expanding clouds through a Stern-Gerlach apparatus [27,28]. Other possible Mott phases, as shown in Fig. 1, are also possible if there is more than one atom per site. These phases can be detected analogously.

On the other hand, if $a_{BF}<a_{FF}$, one may access the (1,1) phase (Fig. 1) with one fermion and one boson per site. Here in the Mott state, we would find two separate clouds for bosons and fermions in the Stern-Gerlach measurement with an antiferromagnetic state for the fermions which can be deduced in the spatial noise correlation measurement. Further, one can now access the superfluid–metal-insulator transition in this system by reducing the depth of the laser producing the optical lattice. The superfluid-insulator transition can be directly accessed by measuring the measurement momentum distribution of the bosons. This provides us a direct measurement of t_B^c. One can now also change η as discussed in the last paragraph and access $t_B^c(\eta)$ for a given λ. This would provide access to a line of constant λ in the phase diagram of Fig. 8.

Another Fermi-Bose mixture which has been realized so far ^{40}K-^{87}Rb mixture [34]. Here one expects $a_{FF} \simeq a_{BB}$ [21] and negative a_{FB} indicating an attractive interaction between bosons and fermions. The magnitude of a_{FB} is also measured in Ref. [34] and is found to be around $3.6a_{FF}$, although with a large (about 40%) uncertainty. In this system, we expect to find Mott phases where two fermionic atoms sit on the same site with $n_0(\lambda)$ bosonic atoms. Such states can also be detected in experiments by passing the expanding clouds through a Stern-Gerlach apparatus as discussed earlier. The superfluid-insulator transition of the bosons can also be accessed by lowering the lattice depth.

In conclusion, we have studied a Bose-Fermi mixture in an optical lattice trapped by an optical trap. We have sketched a generic phase diagram for the possible Mott states of these systems and also studied the superfluid–metal-insulator transition using a slave-rotor mean-field theory. We have also discussed definite experiments that can be performed on specific experimentally realized systems that can probe at least part of the abovementioned phase diagrams.

APPENDIX: COMPARISON OF PHASE DIAGRAMS

In this section, we compare the phase diagram for a single species Mott-Hubbard system obtained using the projection operator with those obtained using mean-field theories [3,5,6] and strong-coupling expansions [26]. To do this, we consider the case of zero coupling between the bosons and fermions ($\lambda=0$). Our starting point is the Bose-Hubbard Hamiltonian of Eq. (21) with $\lambda=0$. By tracing the same set of steps, as in Sec. III A, we then obtain the effective Hamiltonian H^* [Eq. (38)]. The next step is to obtain the variational energy using the wave function Ψ_v [Eq. (40)]. For the purpose of variational energy computations, it is sufficient to consider Ψ_v with real coefficients a, b, and c [Eq. (40)]. This amounts to setting the phase of the superfluid order parameter Δ [Eq. (42)] to zero and does not affect the variational energy. A straightforward calculation then yields

$$E_v = \langle \Psi_v | H^* | \Psi_v \rangle = E_0 + E_1 + E_2, \quad (A1)$$

$$E_0 = \delta E_p b^2 + \delta E_h c^2, \quad (A2)$$

$$E_1 = -zt_B a^2 [(n_0 + 1)b^2 + n_0 c^2], \quad (A3)$$

$$\begin{aligned}
E_2 = &-\frac{zt_B^2 n_0(n_0 + 1)}{U}(a^4 - 2b^2 c^2) \\
&-\frac{z(z-1)t_B^2 n_0(n_0 + 1)}{U}[a^4(b^2 + c^2) - 4a^2 b^2 c^2] \\
&+\frac{2z(z-1)t_B^2 \sqrt{n_0 + 1}}{U}\{2bc[b^2(n_0 + 1) + c^2 n_0] \\
&-(2n_0 + 1)b^2 c^2\}a^2, \quad (A4)
\end{aligned}$$

where $\delta E_p=(-\mu+Un_0)$ and $\delta E_h=[\mu-U(n_0-1)]$ are the on-site energy costs of adding a particle and a hole, respectively, to the Mott phase, and $z=2d$ denotes the coordination number for a d-dimensional hypercubic lattice. The phase diagram can now be obtained by minimizing the variational energy E_v for given $(t_B/U, \mu/U)$. The Mott-superfluid phase boundary then corresponds to the minimum value of $t_c(\mu)$ for which the superfluid order parameter Δ [Eq. (42)] is non-zero. Notice that ignoring the $O(t_B^2/U^2)$ terms amounts to setting $E_2=0$. Our numerical results in this section, however, retain all terms in E_2.

Next, we obtain the expression of t_c^{MF} using mean-field theory. This can be done in a standard manner as shown in

Refs. [3,5,6,37] and the mean-field critical hopping strength in d dimensions can be obtained [37]

$$t_c^{\text{MF}} = \left(\frac{n_0 + 1}{U n_0 - \mu} + \frac{n_0}{\mu - U(n_0 - 1)} \right)^{-1}, \tag{A5}$$

where n_0 denotes the boson occupation number of the Mott phase from which the phase boundary is approached.

Finally, we compare the phase diagram obtained from minimizing the variational energy E_v with the strong-coupling expansion developed in Ref. [26]. The main idea behind the strong-coupling expansion is that at the phase transition point, for a given μ/U, the defect state, which corresponds to an additional particle or hole added to the Mott state, becomes energetically more favorable. Thus, the energy difference of the particle or hole defect states with the Mott state given to $O(t_B^2/U^2)$ by [35]

$$\epsilon_p = \delta E_p - z t_B (n_0 + 1) + \frac{z t_B^2}{2U} (5 n_0 + 4) n_0 - \frac{z^2 t_B^2}{U} n_0 (n_0 + 1), \tag{A6}$$

$$\epsilon_h = \delta E_h - z t_B n_0 + \frac{z t_B^2}{2U} (5 n_0 + 1)(n_0 + 1) - \frac{z^2 t_B^2}{U} n_0 (n_0 + 1) \tag{A7}$$

vanishes at $t_B = t_c^p$ or t_c^h. The phase boundary is obtained by finding the critical hopping $t_c = \min[t_c^p, t_c^h]$.

Before resorting to numerical evaluation of the phase diagram from all different techniques, we would like to clarify the following points. First, although both the defect state calculations of Ref. [26] and the projection operator technique outlined here capture some contributions of t_B^2/U^2 fluctuations, they are not identical to each other. To see this, we consider a second order virtual process for a defect state with one additional particle (hole) $|n_0 + (-)1\rangle_i |n_0\rangle_j \rightarrow |n + (-)2\rangle_i |n - (+)1\rangle_j \rightarrow |n + (-)2\rangle_i |n\rangle_j$, where i and j are nearest-neighbor sites on the square lattice. This process, which after summing over all sites, gives $O(t_B^2/U^2)$ energy contributions $E_p = -z^2 t_B^2 n_0(n_0 + 2)/2U$ for particles and $E_h = -z^2 t_B^2 (n_0^2 - 1)/2U$ for holes. Note that all the states involved in such a process lie outside the low energy manifold and hence are not captured within the projection operator technique even if states with $|n_0 \pm 2\rangle$ are incorporated in the variational wave function [Eq. (40)]. On the other hand, the projection operator technique together with the variational wave functions leads to terms in E_2 [Eq. (A4)] which involves product of states with one additional particle and hole (terms which involve product of the coefficients b and c). These terms, which becomes important mostly near the tip of the Mott lobe, are necessarily absent in defect state calculations in Ref. [26] which considers energy lowering due to a single particle or hole added over the Mott state. Thus we find that the best way to compare different approaches is to compare the phase diagrams obtained using them.

Second, if we neglect the $O(t_B^2/U^2)$ terms, the saddle point equations for b and c can be easily obtained by minimizing the variational energy in Eqs. (A2) and (A3):

$$\left[(n_0 + 1) - \frac{\delta E_p}{z t_B} \right] b = 2(n_0 + 1) b^3 + n_0 c^2 b,$$

$$\left[n_0 - \frac{E_h}{z t_B} \right] c = n_0 c^3 + (n_0 + 1) b^2 c, \tag{A8}$$

where we have used the constraint $a^2 + b^2 + c^2 = 1$. For the Mott phase, the solution to Eq. (A8) is $b = 0 = c$ and $a = 1$. Note that this ensures that the density in the Mott state is pinned to $\langle n \rangle = n_0$. Solutions with nonzero b and c occur when in the SF phase for which $t_B \geq t_c$. We find that in the superfluid phase near the Mott transition line, Eq. (A8) admits the following solutions. For $\mu/U \leq n_0/(2n_0 + 1)$ one gets $t_c = t_c^h = \delta E_h/z n_0$ and

$$c = \frac{1}{\sqrt{2}} \left(1 - \frac{t_c^h}{t_B} \right)^{1/2}, \quad b = 0, \tag{A9}$$

whereas for $\mu/U \geq n_0/(2n_0 + 1)$ one has $t_c = t_c^p = \delta E_p/z(n_0 + 1)$ and

$$b = \frac{1}{\sqrt{2}} \left(1 - \frac{t_c^p}{t_B} \right)^{1/2}, \quad c = 0. \tag{A10}$$

Equations (A9) and (A10) show that near the phase transition $b, c \ll a$, which is crucial to our analysis. Further, as normally expected in a second order quantum phase transition, the coefficients b and c are continuous across the transition. Next, we discuss inclusion of $O(t_B^2/U^2)$ terms. If these terms [Eq. (A4)] are included, obtaining analytical solutions for b and c becomes difficult as it amounts to solving two coupled cubic equations. However, we have checked during numerical evaluation of the phase diagram minimizing Eq. (A1) [which retains second order terms in Eq. (A4)] that b and c are always small compared to a near the phase transition and that near the ends of the Mott lobe their numerical values are well reproduced by Eqs. (A9) and (A10).

Finally, we comment about our choice of variational wave function in which we have only retained states with one additional particle and hole per site over the parent Mott state. In principle, one can retain states with two or more particles per site which leads to a more complicated trial wave function. For example, one can retain the states $|n_0 \pm 2\rangle$ so that the variational wave functions become

$$|\psi'\rangle = \prod_i |\psi'\rangle_i,$$

$$|\psi'\rangle_i = a|n_0\rangle + b|n_0 + 1\rangle + c|n_0 - 1\rangle + d|n_0 + 2\rangle + e|n_0 - 2\rangle, \tag{A11}$$

which leads to a variational energy to $O(t_B/U)$ [Eq. (39)] $E_v' = \langle \psi'|H_0(\lambda = 0) + T^0|\psi'\rangle = E_{0v}' + E_{1v}'$, where

$$E_{0v}' = \delta E_p b^2 + \delta E_h c^2 + \delta E_{2p} d^2 + \delta E_{2h} e^2,$$

$$\delta E_{2p} = -2\mu + U(2n_0 + 1), \quad \delta E_{2h} = 2\mu - 3U(n_0 - 1),$$

$$
\begin{aligned}
E'_{1v} = -\,zt_b\big[&(n_0+1)a^2b^2 + n_0a^2c^2 + (n_0-1)c^2e^2 \\
&+ \sqrt{n_0(n_0-1)}\,c^2ae + \sqrt{(n_0+2)(n_0+1)}\,b^2ad \\
&+ 2\sqrt{(n_0-1)(n_0+2)}\,bcde \\
&+ (n_0+2)d^2b^2 + abc\big(d\sqrt{n_0(n_0+2)} + e\sqrt{n_0^2-1}\big)\big].
\end{aligned}
$$
$$(A12)$$

To analyze the phase diagram obtained from Eqs. (A11) and (A12), we first note that in the Mott phase $a=1$ and $b=c=d=e=0$, as discussed before. Next let us discuss the minimization of E'_v near the Mott-SF transition line. When $d=e=0$, the MI-SF transition occurs at $zt_c=\min(t_c^p, t_c^h)$, with $b, c \ll 1$ and $a \simeq 1$. So to find out whether nonzero d and/or e is favorable for energy minimization, we need to find the effect of turning on a nonzero d and/or e near this transition point and check whether it leads to lowering of the variational energy. We find that turning on a nonzero d and/or e near this point, as can be seen from the expression of E'_{1v} [Eq. (A12)], leads to energy gain $\ll zt_c$ (since in the expression of E'_{1v}, d and e always appear as a product with b and c which are small), whereas the energy cost [Eq. (A11)] is $O(\delta E_{2p})$ and/or $O(\delta E_{2h})$. It turns out that the latter is always greater than the former which leads to a net nonzero energy cost. As a specific example to demonstrate this point, let us consider $\mu \simeq U$ so that for $t_B \simeq t_c = t_c^p$, $b \neq 0$ and $c=0$ [Eq. (A10)]. Then turning on a nonzero d results in an energy change $\delta E = d\{\delta E_{2p}d - zt_c[(n_0+2)b^2d + \sqrt{(n_0+2)(n_0+1)}\,b^2a]\} > 0$ since $b, d \ll 1$ and $\delta E_{2h} - zt_c \simeq U(n_0+1) - \mu > 0$. Thus near $t_B = t_c$, the energy cost from E'_{0v} clearly outweighs energy gain from E'_{1v} (since $zt_c/U \ll 1$ for all parameter regimes and $b, c, d, e \ll 1$ near $t_B = t_c$) and hence the coefficients d and e remain vanishingly small at the phase transition. As we move inside the superfluid phase and t_B becomes large compared to t_c, these coefficients becomes significant. In the present work, we have always restricted ourselves to regions sufficiently near the transition line where the coefficients d and e are small. We note that we have explicitly checked numerically from the full variational energy [including $O(t_B^2/U^2)$ terms which we have not written down explicitly here to avoid clutter], that the abovementioned qualitative argument always holds for all the regimes studied in the present work. We shall therefore neglect these terms in the rest of this section.

To compare the results from different approaches, we now plot the phase diagrams for $n_0=1$ obtained by minimizing the full variational energy E_v to $O(t_B^2/U^2)$ [Eq. (A1)] from the mean-field equation [Eq. (A5)], and by computing the energy of the defect states to $O(t_B^2/U^2)$ [26]. These plots are shown in Fig. 9 for $d=2$ and in Fig. 10 for $d=3$. We find that in spite of the dissimilarity of the two approaches discussed above, the numerical phase boundary obtained by minimizing E_v matches that obtained from the $O(t_B^2/U^2)$ defect state calculation of Ref. [26] quite well in both cases, but differs substantially from the phase boundary obtained using the mean-field theory. Further, for $d=2$, quantum Monte Carlo data, available for the critical hopping at the tip of the Mott lobe [26,36], predicts $(t_c/U)_{MC}=0.061\pm0.006$. The corre-
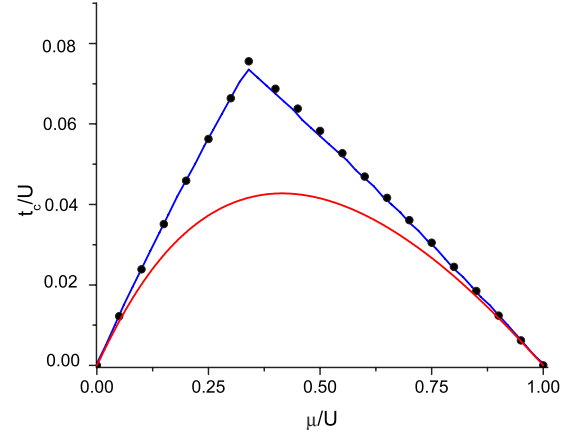

FIG. 9. (Color online) Phase diagram for $d=2$ and $n_0=1$ calculated by minimizing variational energy E_v (black dots), mean-field theory (red solid line), and defect energy calculation to $O(t_B^2/U^2)$ (blue solid line). The phase boundaries computed by minimizing E_v and by defect energy calculations compare well to each other but differ from the mean-field theory near the tip of the Mott lobe.

sponding values obtained from the minimization of E_v and $O(t_B^2/U^2)$ defect state energy calculation of Ref. [26] are $(t_c/U)_{var}=0.0755$ and $(t_c/U)_{defect}=0.0735$, respectively. The mean-field theory predicts a value $(t_c/U)_{MF}=0.041$ while an $O(t_B^3/U^3)$ calculation of defect state energies [26] gives $(t_c/U)_{defect}=0.068$. Thus we conclude that the phase boundary obtained from our variational energy calculation scheme compares well with the defect state energy calculation to $O(t_B^2/U^2)$.

In $d=3$, we can compare our results in Fig. 10 to Figs. 5–7 for $\lambda=0$ and $\mu=0.7$ and $\mu=0.4$, respectively. We find that the phase diagram obtained using the projection operator techniques predicts $t_c/U=0.0232$ for $\mu/U=0.7$ and $\eta=5$ (Fig. 5) and predicts $t_c/U=0.0431$ for $\mu/U=0.4$ and $\eta=4$ (Fig. 7). As seen from Fig. 10, these values compare well to

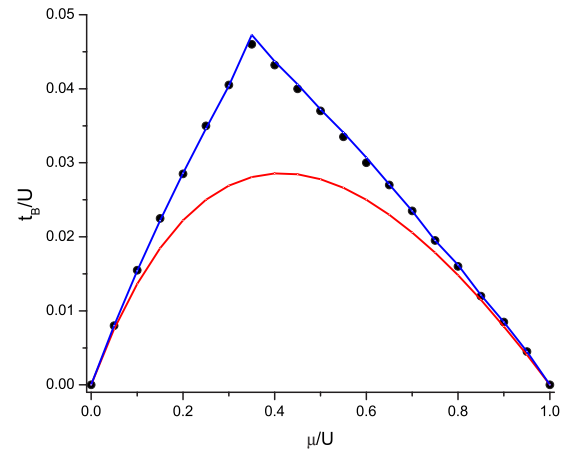FIG. 10. (Color online) Phase diagram for $d=3$ and $n_0=1$. All notations are same in Fig. 9. As in 2D, the phase boundaries computed by minimizing E_v and by defect energy calculations compare well to each other but differ from the mean-field theory near the tip of the Mott lobe.

those obtained from defect state calculations to $O(t_B^2/U^2)$. However, they do not compare favorably with t_c^{MF} which predicts $t_c^{\mathrm{MF}}/U=0.0208$ for $\mu/U=0.7$ and $t_c^{\mathrm{MF}}/U=0.0266$ for $\mu/U=0.4$. Further, the corresponding values of t_c/U from the third order defect state calculation are 0.0225 for $\mu/U=0.7$ and 0.0405 for $\mu/U=0.4$ which compare quite favorably to the projection operator method, but not to the mean-

field theory. At the tip of the Mott lobe ($\mu/U \simeq 0.37$), where the difference between results obtained from different methods become most apparent, the values of t_c/U obtained from different methods are 0.0419 (third order defect state), 0.0459 (second order defect state), 0.0451 (projection operator technique), 0.0276 (mean field), and 0.03480(2) (very recently available quantum Monte Carlo results [38]).

[1] M. Greiner, O. Mandel, T. Esslinger, T. W. Hansch, and I. Bloch, Nature (London) **415**, 39 (2002); M. Greiner, O. Mandel, T. W. Hansch, and I. Bloch, *ibid.* **419**, 51 (2003).

[2] C. Orzel, A. K. Tuchman, M. L. Fenselau, M. Yasuda, and M. A. Kasevich, Science **291**, 2386 (2001).

[3] M. P. A. Fisher, P. B. Weichman, G. Grinstein, and D. S. Fisher, Phys. Rev. B **40**, 546 (1989).

[4] D. Jaksch, C. Bruder, J. I. Cirac, C. W. Gardiner, and P. Zoller, Phys. Rev. Lett. **81**, 3108 (1998).

[5] K. Sheshadri, H. R. Krishnamurthy, R. Pandit, and T. V. Ramakrishnan, Europhys. Lett. **22**, 257 (1993).

[6] D. van Oosten, P. van der Straten, and H. T. C. Stoof, Phys. Rev. A **63**, 053601 (2001).

[7] K. Sengupta and N. Dupuis, Phys. Rev. A **71**, 033629 (2005).

[8] A. Imambekov, M. Lukin, and E. Demler, Phys. Rev. A **68**, 063602 (2003).

[9] A. B. Kuklov and B. V. Svistunov, Phys. Rev. Lett. **90**, 100401 (2003); A. Kuklov, N. Prokofev, and B. Svistunov, *ibid.* **92**, 050402 (2004).

[10] L-M. Duan, E. Demler, and M. D. Lukin, Phys. Rev. Lett. **91**, 090402 (2003).

[11] A. Isacsson, Min-Chul Cha, K. Sengupta, and S. M. Girvin, Phys. Rev. B **72**, 184507 (2005).

[12] M. Greiner, C. A. Regal, and D. S. Jin, Nature (London) **426**, 537 (2003).

[13] M. W. Zwierlein, J. R. Abo-Shaeer, A. Schirotzek, and W. Ketterle, Nature (London) **435**, 1047 (2005).

[14] For a review, see R. Onofrio and C. Presilla, J. Stat. Phys. **115**, 57 (2004).

[15] G. Roati, E. de Mirandes, F. Ferlaino, H. Ott, G. Modugno, and M. Inguscio, Phys. Rev. Lett. **92**, 230402 (2004); G. Modugno, E. de Mirandes, F. Ferlando, H. Ott, G. Roati, and M. Inguscio, in *ATOMIC PHYSICS 19: XIX International Conference on Atomic Physics*, edited by Luis Gustavo Marcassa, Vanderlei Salvador Bagnato, and Kristian Helmerson, AIP Conf. Proc. No. 770 (AIP, Melville, NY, 2005), p. 197.

[16] R. Roth and K. Burnett, Phys. Rev. A **69**, 021601(R) (2004).

[17] A. Albus, F. Illuminati, and J. Eisert, Phys. Rev. A **68**, 023606 (2003).

[18] M. Lewenstein, L. Santos, M. A. Baranov, and H. Fehrmann, Phys. Rev. Lett. **92**, 050401 (2004).

[19] M. Cramer, J. Eisert, and F. Illuminati, Phys. Rev. Lett. **93**, 190405 (2004).

[20] Y. Yu and S. T. Chui, Phys. Rev. A **71**, 033608 (2005).

[21] F. Illuminati and A. Albus, Phys. Rev. Lett. **93**, 090406 (2004).

[22] L. D. Carr and M. J. Holland, Phys. Rev. A **72**, 031604 (2005).

[23] More precisely, this means that the fermions in the mixture are of the same species but can belong to two different total angular momentum (or generalized spin) states [21].

[24] S. Florens and A. Georges, Phys. Rev. B **70**, 035114 (2004); A. Georges, S. Florens, and T. A. Costi, J. Phys. IV **114**, 165 (2004).

[25] C. Schroll, F. Marquardt, and C. Bruder, Phys. Rev. A **70**, 053609 (2004).

[26] J. K. Freericks and H. Monien, Europhys. Lett. **26**, 545 (1994); Phys. Rev. B **53**, 2691 (1996).

[27] J. Stegner *et al.*, Nature (London) **396**, 345 (1998).

[28] J. Widera *et al.*, Phys. Rev. Lett. **95**, 190405 (2005).

[29] E. Altman, E. Demler, and M. D. Lukin, Phys. Rev. A **70**, 013603 (2004).

[30] M. Greiner, C. A. Regal, J. T. Stewart, and D. S. Jin, Phys. Rev. Lett. **94**, 110401 (2005).

[31] A. G. Truscott *et al.*, Science **291**, 2570 (2004).

[32] F. Schreck, L. Khaykovich, K. L. Corwin, G. Ferrari, T. Bourdel, J. Cubizolles, and C. Salomon, Phys. Rev. Lett. **87**, 080403 (2001).

[33] Such a variation also changes U_{FF}/U_{BB} in principle. But one can achieve an appreciable change in η by maintaining a small change in U_{FF}/U_{BB} since t_F has an exponential dependence on the lattice potential.

[34] G. Roati, F. Riboli, G. Modugno, and M. Inguscio, Phys. Rev. Lett. **89**, 150403 (2002); F. Ferlaino, C. D'Errico, G. Roati, M. Zaccanti, M. Inguscio, G. Modugno, and A. Simoni, Phys. Rev. A **73**, 040702(R) (2006).

[35] The defect state energies are calculated to $O(t_B^3/U^3)$ in Ref. [26]. Here we have only retained terms to $O(t_B^2/U^2)$ for the purpose of comparison with our approach in Figs. 9 and 10.

[36] W. Krauth and N. Trivedi, Europhys. Lett. **14**, 627 (1991); W. Krauth, N. Trivedi, and D. Ceperley, Phys. Rev. Lett. **67**, 2307 (1991).

[37] S. Sachdev, *Quantum Phase Transitions* (Cambridge University Press, Cambridge, UK, 1999).

[38] B. Caprogrosso-Sansone, N. Prokof'ev, and B. V. Svistunov, e-print arXiv:cond-mat/0701178 (unpublished).